Science and Engineering Research Council
Rutherford Appleton Laboratory
CHILTON, DIDCOT, OXON, OX11 0QX

RAL-86-019

The ISIS Time Focussed Crystal Analyser Spectrometer, TFXA.

J. Penfold and J. Tomkinson.

February 1986

THE ISIS TIME FOCUSSED CRYSTAL ANALYSER SPECTROMETER, TFXA

J Penfold and J Tomkinson

Abstract

The design and performance of a time focussed crystal analyser spectrometer, which has been installed on the ISIS spallation neutron source, is presented.

The combination of time and energy focussing provides good (~ 2 to 3%) energy transfer resolution over a wide range of energy transfers (10 to 500 meV).

Initial results from zirconium hydride and potassium hydrogen maleate demonstrate clearly the good energy transfer resolution, and show an excellent signal to noise ratio.

Further potential improvements in both count rate and resolution are discussed.

Neutron Division
Rutherford Appleton Laboratory
Chilton
Didcot
Oxon OX11 0QX
UK

February 1986

CONTENTS :

1. INTRODUCTION

The time focussed crystal analyser TFXA is an indirect geometry time of flight inelastic scattering spectrometer, using a time-focussed pyrolytic graphite analyser to give good count rates, and good energy transfer resolution over a wide range of energy transfers.

Many designs of inverse geometry crystal analyser spectrometers have demonstrated good energy resolution (1-5). More recently Ikeda et al (6-7) have constructed an inverse geometry crystal analyser spectrometer with a time focussed arrangement, in which the sample and detector arrays are in the same plane, and the analysing crystal is set parallel to this plane. In such a geometry, for an ideal crystal, all detected neutrons have the same flight time after scattering. The TFXA spectrometer is based on the focussing geometry of Ikeda et al.

In addition to the time focussing, the Marx principle is used to provide energy focussing (8). This reduces the positional uncertainty in the analysing energy, E_2, and is a feature not previously exploited on crystal analyser spectrometers. It enables the good energy transfer resolution to be maintained down to energy transfers of a few meV.

As the energy of the detected neutrons is small compared to incident energy, their scattering vector is practically independent of scattering angle. Thus, there can be little variation in momentum transfer, $\hbar Q$, independent of energy transfer. This is relatively unimportant in molecular vibrational spectroscopy, where the dispersion of the vibrational mode is small or cannot be easily studied. TFXA has been designed for the study of vibrational spectroscopy of incoherent scatterers and polycrystalline samples, to complement the traditional infrared and Raman techniques in chemistry, physics and materials science.

The need for high resolution in vibrational spectroscopy has been clearly demonstrated by Ikeda et al (6,7) for hydrogen in metal systems and for molecular spectroscopy by Lauter and Jobic (9). The TFXA spectrometer has therefore been designed to be competitive in resolution and signal/noise to recent instrumental developments in crystal analysers (6,7), reactor (9) and pulsed source (10) based filter techniques.

The crystal analyser offers distinct advantages in terms of resolution, lineshape and signal/noise over filter based techniques. The pulsed source application offers the advantage of the simultaneous measurement of the whole energy transfer range to higher values of energy transfers, with significantly more flux at the higher energies than the reactor based instruments.

We discuss in this paper the design and calculated performance of the spectrometer. Initial commissioning results on zirconium hydride and potassium hydrogen maleate are presented, and show excellent characteristics with respect to resolution and signal/noise.

Some forthcoming improvements in both count rate and resolution are discussed.

2. INSTRUMENT DESIGN AND CALCULATED PERFORMANCE

A general expression for the energy transfer resolution of inverse geometry inelastic spectrometers can be written approximately as

$$\frac{\Delta\hbar\omega}{\hbar\omega} = \frac{1}{\hbar\omega}\{((\partial\hbar\omega/\partial E_2)^2 + ((\partial\hbar\omega/\partial L_2)\Delta L_2)^2 + ((\partial\hbar\omega/\partial t)\Delta t)^2 + ((\partial\hbar\omega/\partial L_1)\Delta L_1)^2\}^{\frac{1}{2}} \quad (1)$$

where,

$$\frac{\partial\hbar\omega}{\partial E_2} = [1 + L_2/L_1(E_1/E_2)^{3/2}] \quad (2)$$

$$\frac{\partial\hbar\omega}{\partial L_2} = 2E_1^{3/2}/L_1E_2^{\frac{1}{2}} \quad (3)$$

$$\frac{\partial\hbar\omega}{\partial t} = 2E_1^{3/2}/AL_1 \quad (4)$$

$$\frac{\partial\hbar\omega}{\partial L_1} = \frac{2E_1}{L_1} \quad (5)$$

$$\Delta t = (\Delta t_m 2 + \Delta t_{ch} 2)^{\frac{1}{2}} \quad (6)$$

$\hbar\omega$ is the energy transfer, E_1 is the incident energy, E_2 the analysis energy, ΔE_2 the band pass of the analyser, L_1 and L_2 the incident and scattered flight paths, ΔL_1 and ΔL_2 the distribution of incident and scattered flight paths, Δt_m the pulse width from the moderator, Δt_{ch} the time of flight channel width, and A is a constant.

The energy transfer resolution is generally dominated by the band pass of the analyser, ΔE_2, with a smaller contribution from the distribution of secondary flight paths. Apart from reducing ΔE_2, it is important that L_2/L_1 is small; as there are limits to the reduction in L_2 for most practical analyser systems, generally L_1 must be larger.

If the energy analysis is made by Bragg reflection from a crystal, using the time focussed geometry described in references 6 and 7 and shown schematically in figure 1, for an ideal crystal all detected neutrons have the same secondary flight time. To first order it has been shown that (6-8,11) the crystal mosaic of the analyser does not affect the focussing. The ΔE_2 contribution to the energy transfer resolution then reduces to $\partial\hbar\omega/\partial E_2 = 1.0$. It is now no longer necessary to reduce the L_2/L_1 ratio, and, as the other terms which depend on L_1 are in general smaller, L_1 can be reduced without appreciably affecting the resolution. A reduction in L_1 can therefore partially compensate for the smaller solid angle a crystal analyser may easily cover with respect to filter type analysers.

ΔE_2 is now given by,

$$\Delta E_2 = 2E_2 \cot \theta_A \, \Delta\theta_A \qquad (7)$$

where E_2 is the analysing energy and θ_A is the analyser Bragg angle.

If the detector array is taken as a whole, then the angle subtended between the analyser and the detector is greater than that subtended between the sample and analyser, consequently $\Delta\theta_A$ is effectively the angle subtended between the sample and the analyser. If, however, the detector array is of the form of a one dimensional position sensitive detector then the Marx principle can be applied to remove the positional uncertainty in the analysing energy, E_2. Each detector element, dx, will be associated with a different value of E_2 given by,

$$E_2 = \frac{(h^2 + x^2/4)}{B^2h^2} \tag{8}$$

where h is the distance between the sample and the detector planes, x the position along the detector, and B is a constant.

ΔE_2 is now given by,

$$\Delta E_2 = \frac{x}{2B^2h^2} \Delta x_r \tag{9}$$

where Δx_r is not the detector element width, but the effective width given by the convolution of the detector element and sample widths, $\Delta x_r = (\Delta x^2 + \Delta s^2)^{\frac{1}{2}}$, Δs is the sample width, and Δx the detector element width.

For determining the resolution the magnitude of ΔE_2 is determined by $\Delta\theta_A$; whereas for intensity considerations it is the crystal mosaic, η, which is important. Within the limits of retaining the same crystal reflectivity, and time focussing being independent of mosaic, increasing the crystal mosaic will increase the detected intensity.

In the secondary flight path the time focussing removes the contributions to resolution from path differences due to finite collimation. The contribution from the distribution of secondary flight paths is now due to detector, sample and analysing crystal thicknesses. It is, therefore, more convenient to write the second term of equation 1 as.

$$\frac{\partial h\omega}{\partial h} \Delta h = \frac{4E_1^{3/2}}{L_1 E_2^{\frac{1}{2}}} \frac{\Delta h}{\sin\theta^A} \tag{10}$$

where,

$$\Delta h = [\Delta d_s^2 + \Delta d_d^2 + \Delta d_a^2]^{\frac{1}{2}} \tag{11}$$

and Δd_s, Δd_d and Δd_a are the effective sample, detector, and analyser thicknesses.

Figure 2 shows the individual contributions to the energy transfer resolution, calculated for the TFXA spectrometer. At low energy transfers ($\leq$ 100 meV) the dominant term is ΔE_2; its contribution is significantly reduced if energy focussing is incorporated. At higher energies the resolution is dominated by the distribution of secondary flight paths, Δh, due to detector, sample and analyser thicknesses. The most significant contribution is from the path length in the current detector system, 2.54 cm BF_3 gas tubes. The reduction in the contribution to the overall resolution by replacing the existing detector system by a thin scintillator detector is clearly seen in figure 2. Figure 3 shows the resulting resolution for TFXA with 2.54 cm BF_3 detectors, with and without energy focussing, and for a TFXA with a thin scintillator detector with energy focussing. The current resolution performance should be $\sim$ 2 to 3% over the energy range of 10 to 500 meV, with an eventual resolution $\sim$ 1% over a wider range of energy transfers if the detector thickness contribution to the secondary flight path distribution is significantly reduced. Beyond that level further improvements in resolution can only be achieved by increasing the primary flight path; if, for example, L_1 was increased from 12.0 to 20.0m then the resolution would be $\leq$ 0.5% from 10 to 1000 meV in energy transfer.

The crystal analyser spectrometer is situated on the ambient beam, N8, at a distance of 12m from the ambient moderator of the ISIS pulsed source, Rutherford Appleton Laboratory. Standard collimation design illuminates a sample area of 50(V) x 25(H) mm^2. The layout of the spectrometer is shown in figure 4. The time focussed geometry used by Ikeda et al (6,7) is adopted where the sample and detector arrays are in the same plane and the crystal analyser is in a parallel plane. The design accommodates two analyser systems placed symmetrically about the sample position, at a scattering angle of 133°. The analyser is a pyrolytic graphite crystal (80 x 80 x 2 mm) with a mosaic spread of 2.5°, and set at a Bragg angle of 43°; giving a final energy, E_2, of 3.9 meV for the $\langle 002 \rangle$ reflection. The important dimensions of the spectrometer are then determined by the Bragg angle of the analyser, the desire to reduce the sample to analyser and analyser to detector distances such that the solid angle is maximised whilst retaining sufficient space for the Beryllium filter, adequate shielding and other mechanical considerations. The distance between the sample/detector and analyser planes is 238 mm. The flight tubes and sample space are comprised within a single cryogenic vacuum. Separated

from this, by a thin aluminium foil window, is the vacuum which houses the crystal analyser and Beryllium filter. The shielding in the immediate vicinity of the vacuum spaces and detector arrays is B_4C/resin. Shielding outside that region is designed to have a minimum of 300 mm of borax/wax. The initial detector system is 16 x 2.54 cm BF_3 gas detectors. Time sorted Li^6 scintillation monitor detectors are sited before and after the spectrometer flight tube flanges. A 150 mm Beryllium filter, cooled to 60K by a closed cycle refrigerator, is sited between the analyser and detectors to surpress higher order reflections from the pyrolytic graphite analyser.

A summary of the important instrumental parameters is listed in table 1.

TABLE 1

Energy analyser	⟨002⟩, pyrolytic graphite, 2θ=43° $\overline{E}_2$ = 3.95 meV dimension = 80 x 80 x 2 mm mosaic spread = 2.5°
Sample size	50(V) x 25(H) mm^2
Incident flight path	L_1 = 12.0m
Secondary flight path	$\overline{L}_2$ = 0.7m
Detectors	16 2.54 cm BF_3 gas detectors area = 2_{off} (160 x 170) mm^2 solid angle 0.12 steradians

3. INITIAL EXPERIMENTAL RESULTS

During the commissioning of TFXA on ISIS at low levels of mean current, spectra of zirconium hydride and potassium hydrogen maleate have been measured.

Figure 5 shows raw time of flight data for zirconium hydride at $\geq$ 70K, for the eight individual detectors viewing one analyser. Each detector has a different final energy, the origin of energy focussing, hence the position of the elastic line in time of flight differs from detector to detector. The variation in time of flight position of inelastic features varies less with increasing energy transfer. This is clearly demonstrated in figure 5. Hence the incorporation of energy focussing means converting each individual spectrum (detector) to an energy transfer scale before they may all be added together.

The use of a well characterised inelastic spectrum enables the calibration of each E_2 and L_2 value associated with the individual detectors to be obtained from the relative positions of the elastic and known inelastic features.

Early calibration using the 140 meV transition of ZrH_2 has been further refined using the 46.87 meV transition in hexamethylene tetramine (HMT) (12). The final energy E_2 varies from 3.0 to 4.8 meV, and t_2 is in the region of 805 μsec. The elastic lines of ZrH_2 and hexamethylene tetramine have been located at zero energy transfer to within 10 μvolts; and are described by a gaussian of fwhm 0.25 meV, in excellent agreement with the calculated elastic resolution. The 46.87 meV transition in HMT has a width = 1.12 meV, and is slightly broader than the calculated resolution at this energy transfer (0.82 meV), but narrower than previously observed (9). Errors in calibration of a peak position are estimated to be $\leq$ 0.5%.

The elastic line of the zirconium hydride, comprising the appropriate sum of all the individual detectors, is shown in figure 6 as a function of energy transfer: the gaussian fit to the lineshape is described by the solid line. In figure 6b an expanded scale of the elastic line shows the characteristic wings of thermal diffuse scattering. Some consideration of the gains which may accrue from cooling the analysing crystals is in progress.

Following the arguments of Ikeda et al (6,7) there is no evidence of the third order reflection for the graphite analyser, which should be the most intense: hence we conclude that higher order surpression is excellent.

Figure 7 shows data proportional to $S(Q,\omega)$ as a function of energy transfer for zirconium hydride at $\geq$ 70K. The insets show the fundamental mode and first overtones on an expanded scale. The good resolution reveals a structure consistent with that reported by Couch, Harling and Clune (13), and Ikeda et al (6,7). Table 2 shows the ratios of integrated intensities for the elastic line, fundamental, first and second overtones; good agreement with harmonic oscillator theory is obtained for the inelastic ratios. The discrepancies involving the elastic intensity are probably due to multiple scattering.

TABLE 2

Ratio	Theoretical	Measured
fundamental/elastic	0.358	0.49 ± 0.03
1st overtone/fundamental	0.739	0.77 ± 0.05
2nd overtone/1st overtone	0.829	0.84 ± 0.10

A detailed analysis of the zirconium hydride data is in progress in conjunction with the complementary data obtained on the direct geometry chopper spectrometer, HET, at ISIS.

Figure 8 shows data proportional to $S(Q,\omega)$ as a function of energy transfer for potassium hydrogen maleate at $\geq$ 70K. The insets show different energy transfer regions on an expanded scale. Particularly noticeable is the contribution of the background to the total intensity. The background appears to remain smooth and flat up to energy transfers of about 250 meV. Compared with other neutron spectra of potassium hydrogen maleate reported in the literature (14,15) a vastly richer structure is obtained. The detail of the spectrum compares favourably with the latest optical data (16). Data analysis is proceeding using recent developments in a refinable normal coordinate program (17).

The results of other commissioning experiments on the spectrometer will be reported in detail elsewhere.

4. CONCLUSIONS

The TFXA spectrometer has shown excellent performance during its commissioning on the ISIS spallation neutron source, with good energy transfer resolution and a good signal to noise ratio. It has the potential to make a significant contribution to neutron vibrational spectroscopy.

ACKNOWLEDGEMENTS

We wish to thank D K Ross for numerous informative discussions, and much useful advice. One of us (JP) would particularly like to acknowledge invaluable assistance from K Crawford during the early stages of the spectrometer design.

The installation effort of the Neutron and ISIS Divisions at RAL, and especially of M Lobo and I Davidson, was much appreciated.

FIGURES

1. Principle of the time focussed crystal analyser.

2. Contributions to the energy transfer resolution, $\Delta\hbar\omega/\hbar\omega$, from Δt, ΔL_1, ΔL_2, and ΔE_2, as a function of energy transfer, $\hbar\omega$.

3. TFXA energy transfer resolution, $\Delta\hbar\omega/\hbar\omega$, as a function of energy transfer.

4. Design of the ISIS time focussed crystal analyser, TFXA.

5. Raw time of flight data for the eight individual detectors which view one analyser, for zirconium hydride at $\geqslant$ 70K.

6. Elastic line for zirconium hydride at $\geqslant$ 70K as a function of energy transfer, $\hbar\omega$.

7. Intensity proportional to $S(Q,\omega)$ as a function of energy transfer, $\hbar\omega$, for zirconium hydride at $\geqslant$ 70K.

8. As (7), but for potassium hydrogen maleate at $\geqslant$ 70K.

REFERENCES

1. P H Day and R N Sinclair, J Chem Phys 55 2807 (1971)

2. S H Chen, J D Jorgensen and C V Berney, J Chem Phys 68 209 (1978)

3. K Skold, K Crawford and S H Clen, Nucl Inst & Meth 145 115 (1977)

4. K Parlinski, M Sudnik-Hrynkiewicz, A Bajorek, J A Janik and W Olejarczyk, Res Appl of Nucl Pulsed Systems IAEA Vienna 197 (1967)

5. D K Ross - unpublished work.

6. S Ikeda, N Watanabe and K Kai, Physica 120B 131 (1983)

7. S Ikeda, N Watanabe, Nucl Inst & Meth 221 571 (1984)

8. D K Ross - private communication

9. H J Lauter and H Jobic, Chem Phys Letters 108 393 (1984)

10. A D Taylor, E J Wood, J A Goldstone and J Eckert, Nucl Inst & Meth 221 408 (1984)

11. K Crawford - private communication

12. M N Thomas and R E Ghosh - Mol Phys 5 1489 (1975)

13. J G Couch, O Harling and C Clune, Phys Rev B 4 2675 (1971)

14. J Tomkinson, I J Braid, J Howard and T C Waddington, Chem Phys 64 151 (1982)

15. J Howard, J Tomkinson, J Eckert, J A Goldstone and A D Taylor, J Chem Phys 78 3190 (1983)

16. F Avbelj, B Orel and D Hadiz, Spect Acta 41A 83 (1984)

17. G J Kearley, J Chem Soc Faraday Trans II 82 41 (1986)

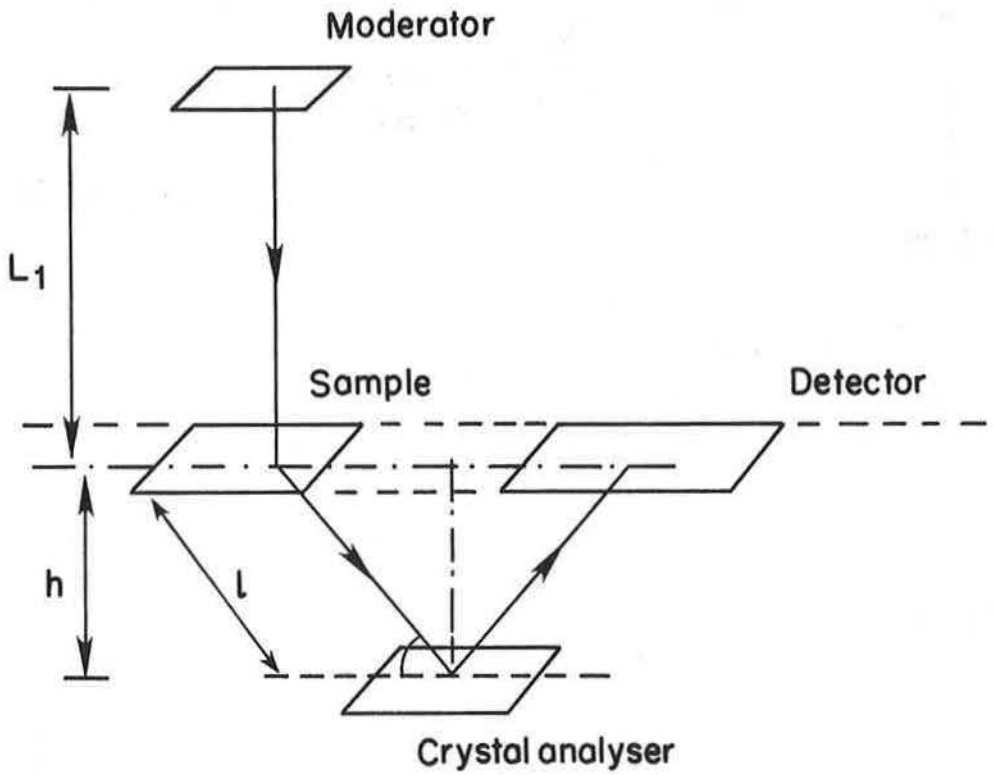

Figure 1.

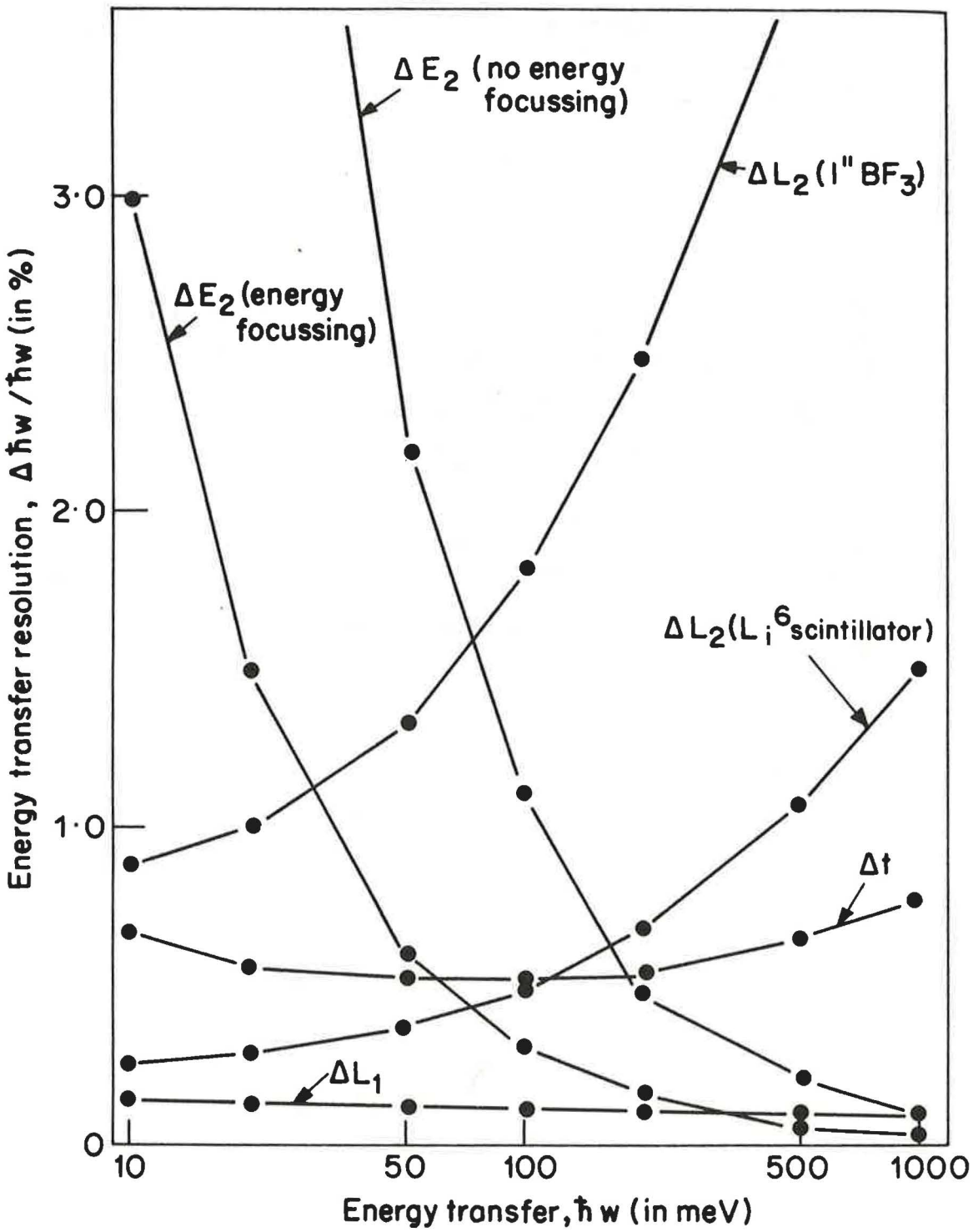
ΔE2 (no energy focussing)
ΔL2 (1" BF3)
ΔE2 (energy focussing)
ΔL2 (Li6 scintillator)
Δt
ΔL1
3·0
2·0
1·0
0
10
50
100
500
1000
Energy transfer resolution, Δħw/ħw (in %)
Energy transfer, ħw (in meV)

Figure 2.

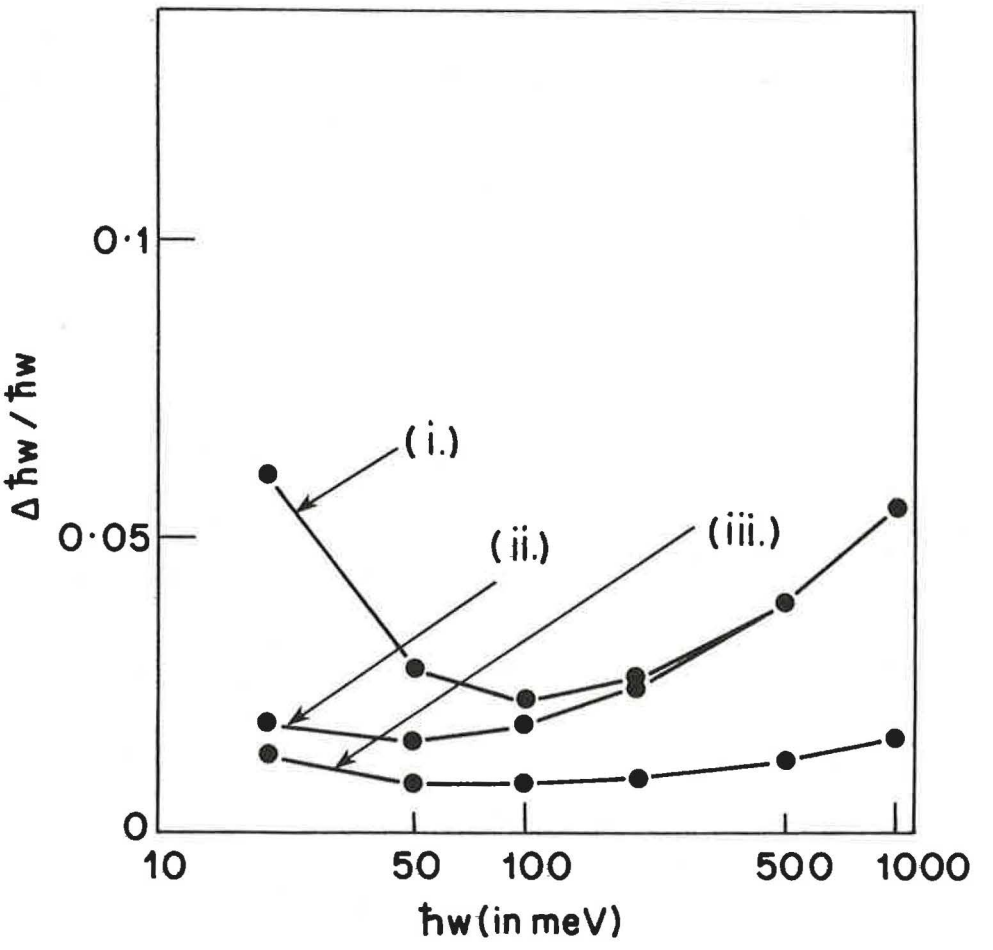

Figure 3.

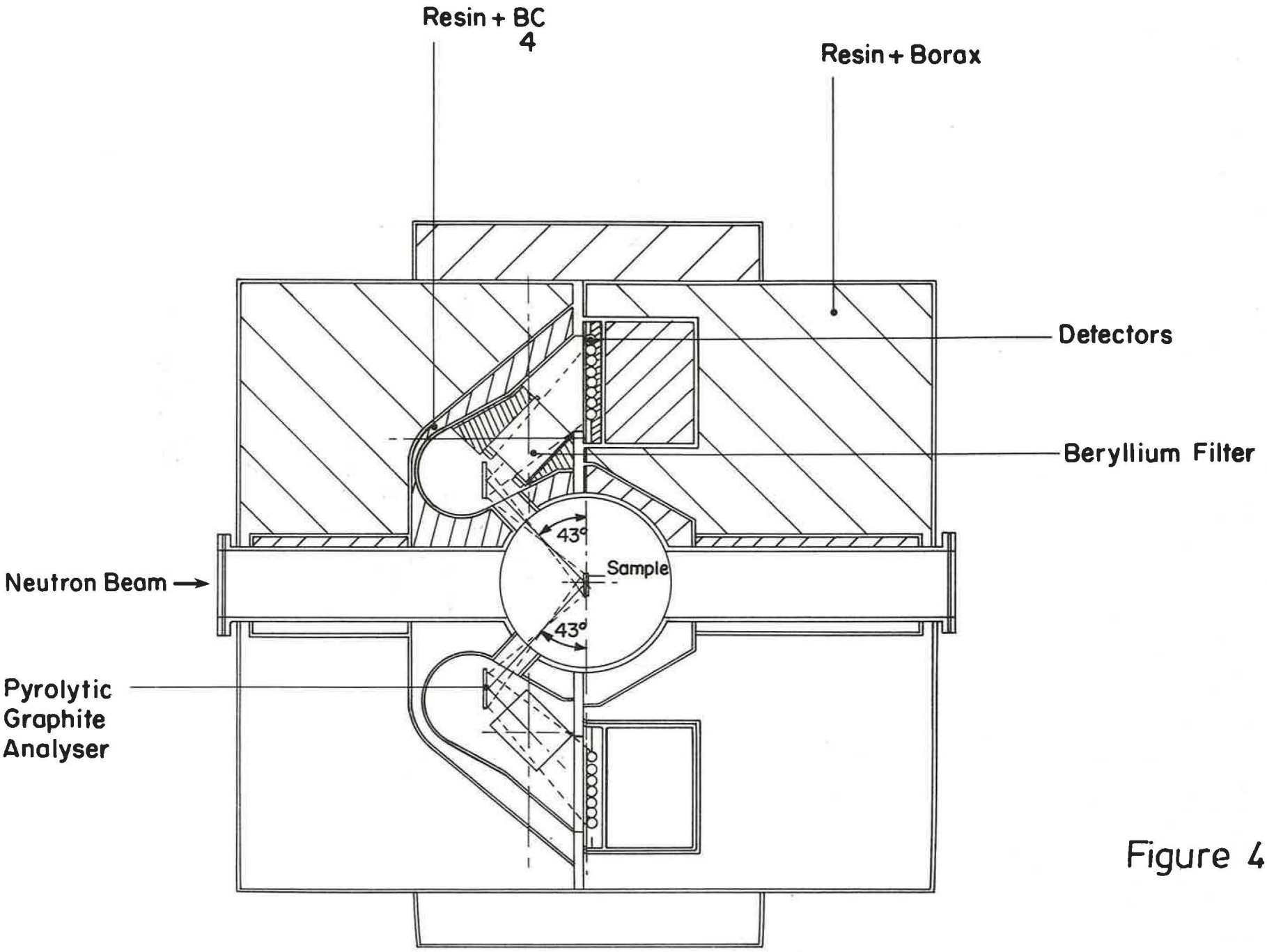
Resin + BC 4
Resin + Borax
Detectors
Beryllium Filter
43°
Sample
43°
Neutron Beam
Pyrolytic Graphite Analyser

Figure 4.

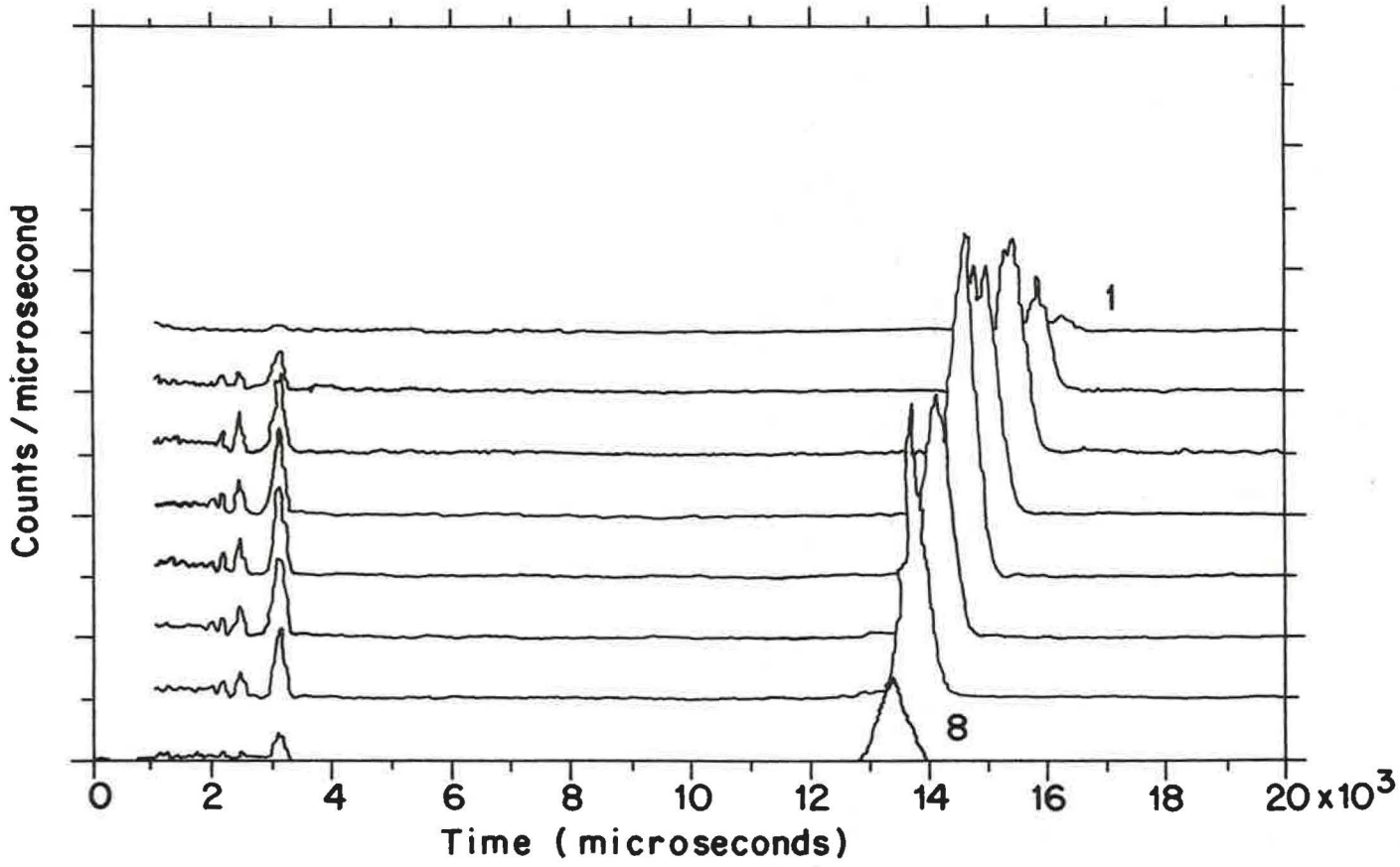
Counts / microsecond
1
8
0
2
4
6
8
10
12
14
16
18
20 x 10^3
Time (microseconds)

Figure 5.

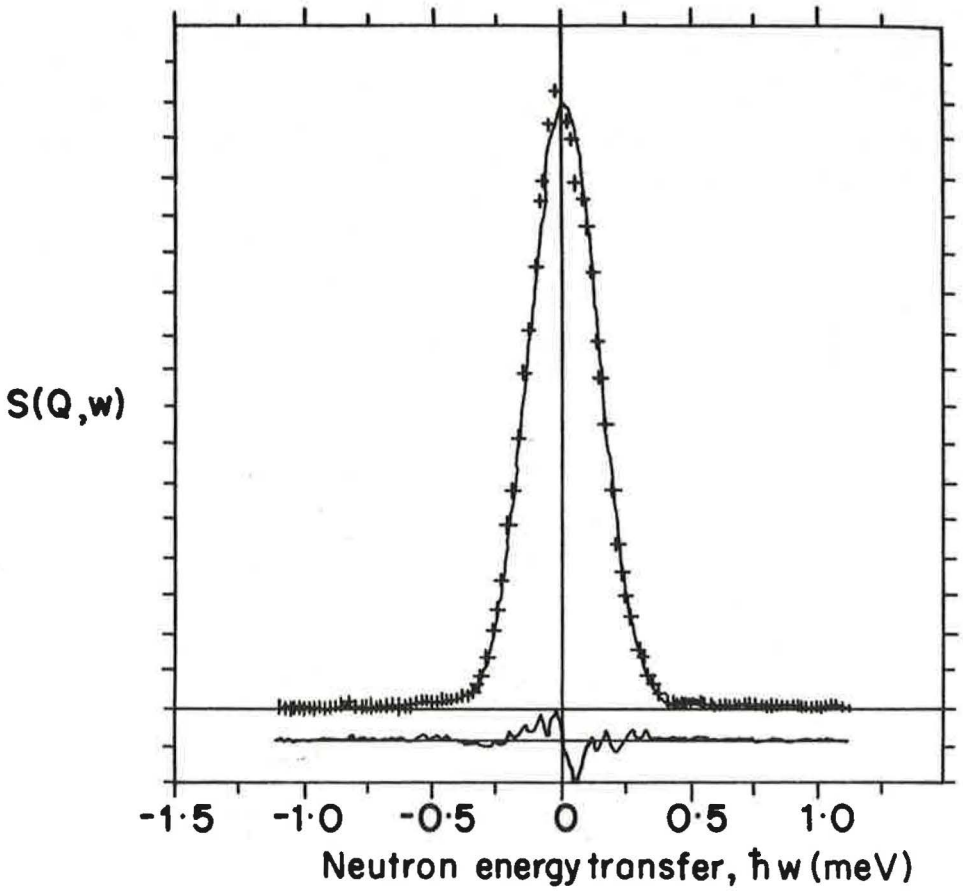
S(Q,w)
-1·5
-1·0
-0·5
0
0·5
1·0
Neutron energy transfer, ħw (meV)
(a)

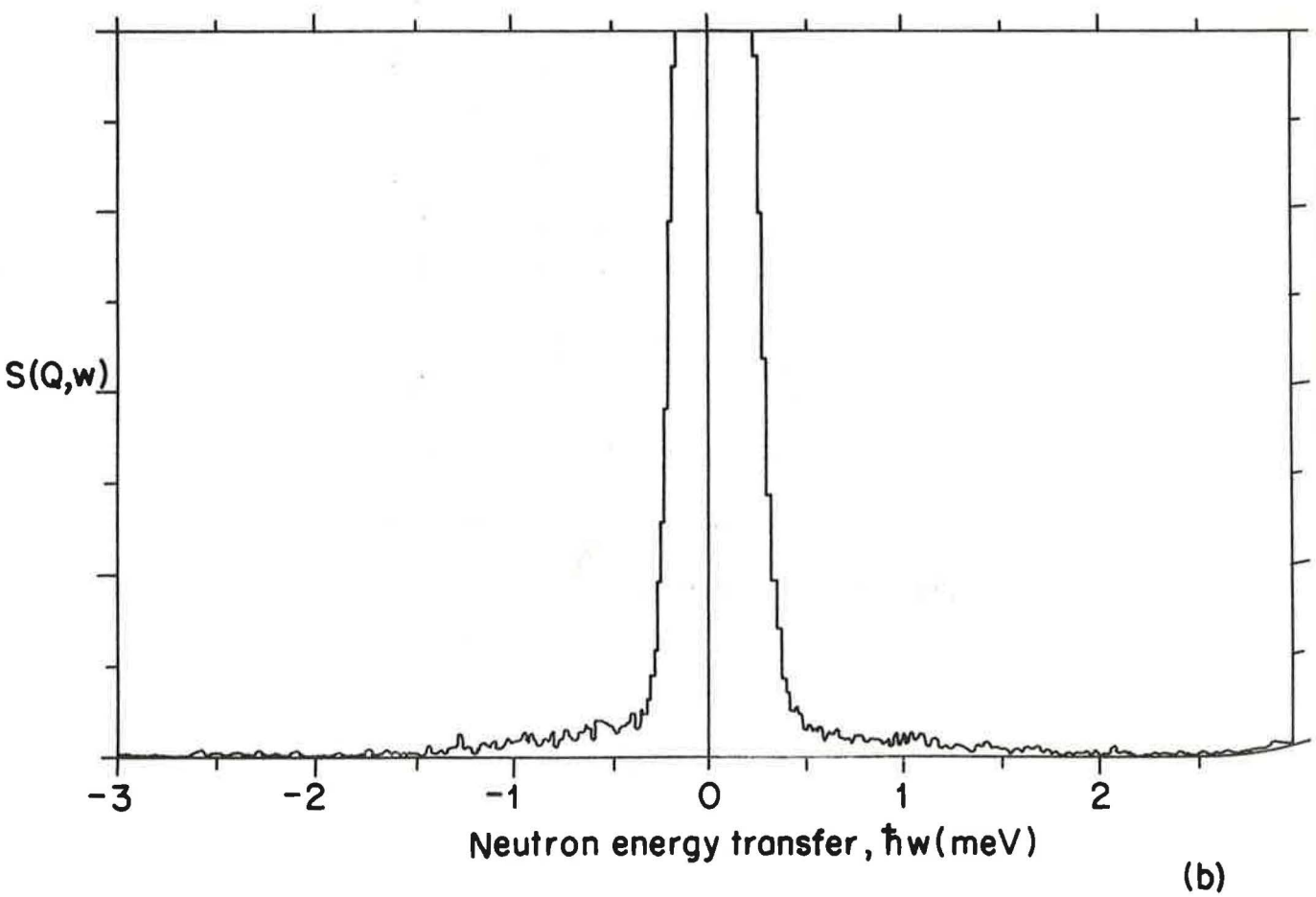
S(Q,w)
-3
-2
-1
0
1
2
Neutron energy transfer, ħw(meV)
(b)

Figure 6

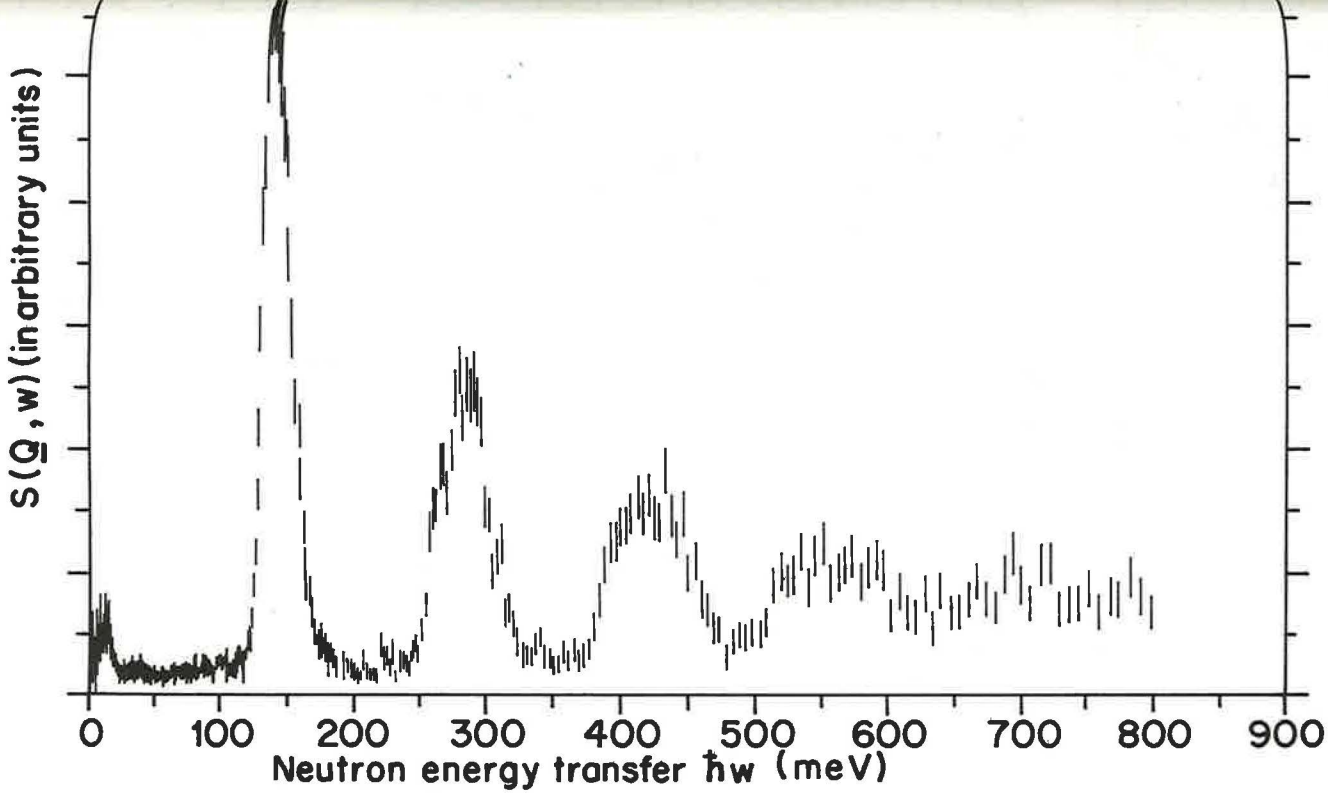
S(Q, w) (in arbitrary units)
0
100
200
300
400
500
600
700
800
900
Neutron energy transfer ħw (meV)

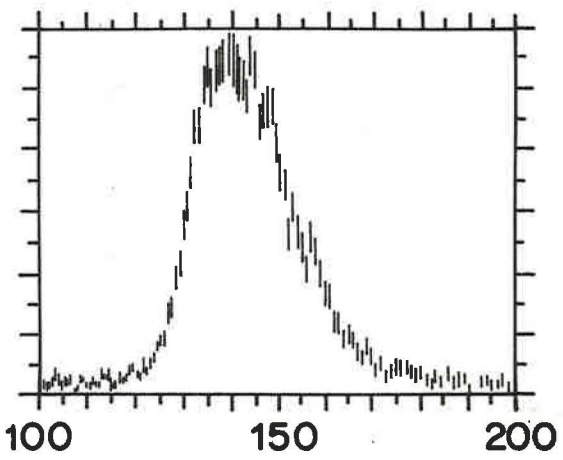
100
150
200

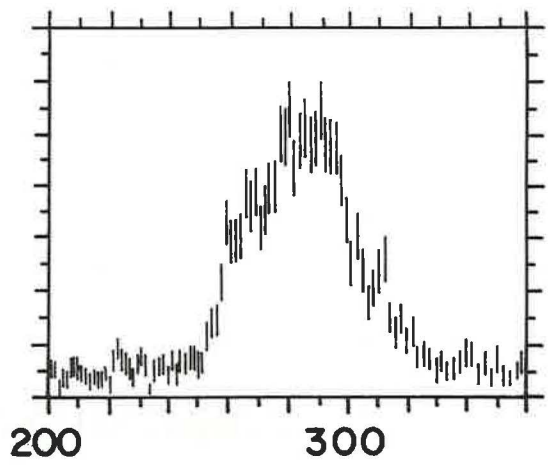
200
300

Figure 7.

Figure 8.

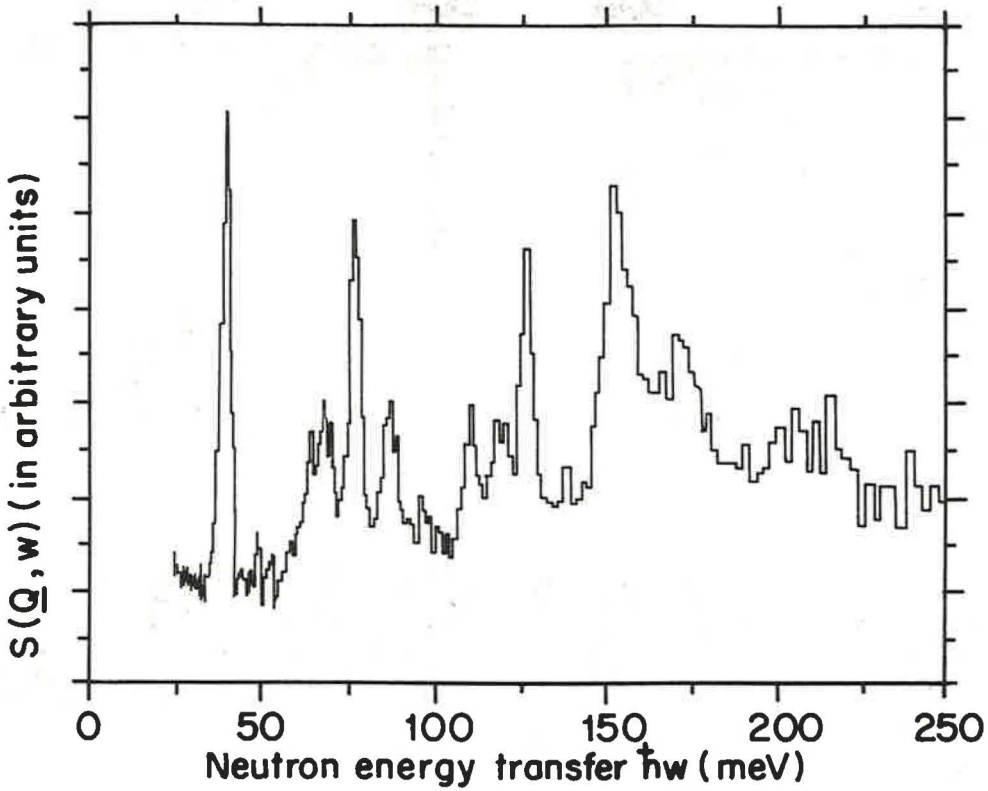
S(Q, w) (in arbitrary units)
0
50
100
150
200
250
Neutron energy transfer ħw (meV)

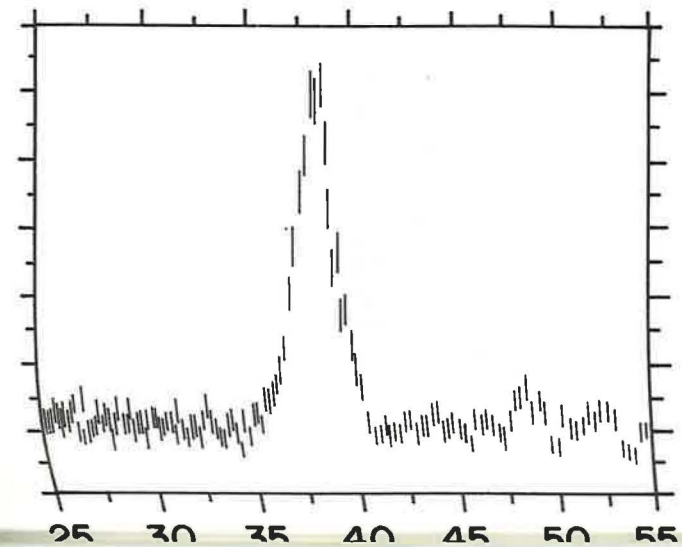
25
30
35
40
45
50
55

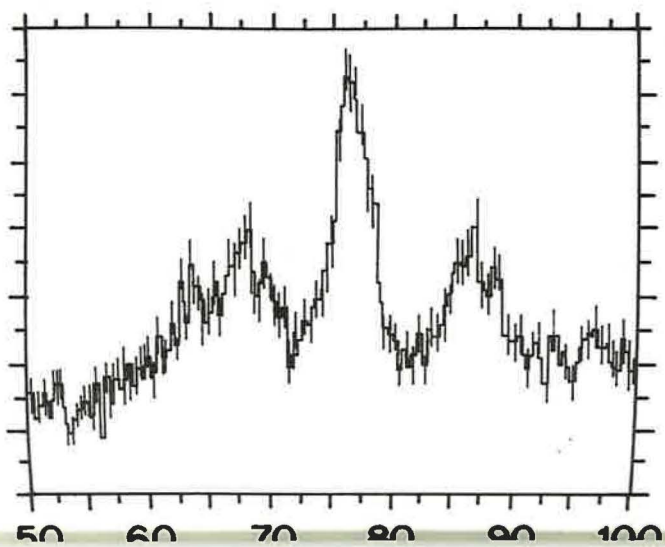
50
60
70
80
90
100

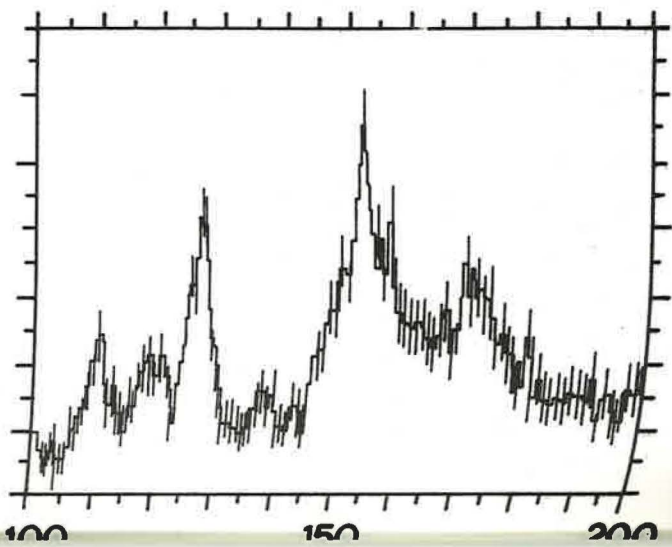
100
150
200